Available online at www.sciencedirect.com

ScienceDirect

www.elsevier.com/locate/jes

JES JOURNAL OF ENVIRONMENTAL SCIENCES

www.jesc.ac.cn

Oxidative degradation of phenol by sulfidated zero valent iron under aerobic conditions: The effect of oxalate and tripolyphosphate ligands

Xianglong Kong[1,2,3], *Chengwu Zhang*[1,2,3], *Jingyi Zhang*[1,2,3], *Lishuang Xuan*[1,2,3], *Chuanyu Qin*[1,2,3,*]

[a] *Key Laboratory of Groundwater Resources and Environment, Ministry of Education, Jilin University, Changchun 130021, China*

[b] *Jilin Provincial Key Laboratory of Water Resources and Environment, Jilin University, Changchun 130021, China*

[c] *National and Local Joint Engineering Laboratory for Petrochemical Contaminated Site Control and Remediation Technology, Jilin University, Changchun 130021, China*

ARTICLE INFO

Article history:
Received 18 January 2020
Revised 16 July 2020
Accepted 16 July 2020
Available online 24 July 2020

Keywords:
Zero valent iron
Sulfidation
Tripolyphosphate
Oxalate
Oxygen activation

ABSTRACT

After adding either organic or inorganic ligands, sulfidated nano-zero-valent iron (SnZVI) was used for aerobic degradation of phenol, and the effect of the ligand species on oxidation performance was investigated. We found that SnZVI hardly degraded phenol in the absence of ligand addition. Ligands initiated and promoted the degradation of pollutants by SnZVI. The data herein show that a characteristic inorganic ligand, tripolyphosphate (TPP), is more effective in enhancing oxidation than a characteristic organic ligand oxalate. In addition to the scavenging of reactive oxidants by the organic ligand, more ferrous ion (Fe(II)) dissolution from SnZVI in the TPP system is another cause for the superior enhancement by the inorganic ligand. In the oxalate system, as the sulfur content of SnZVI increased, the oxidation efficiency increased because FeS shell promoted the transfer of electrons to produce more reactive oxygen species (ROS). In TPP system, the effect of sulfur content on oxidation performance is more complex. The SnZVI with low sulfur content showed poor oxidation performance compared with that of nZVI. Further experiments proved that sulfidation might weaken the complexation of TPP with surface bound Fe, which would slow down the ionic Fe(II) dissolution rate. Therefore, sulfidation has the dual effects of enhancing electron transfer and inhibiting the complexation of inorganic ligands. In addition, the mechanisms of ROS generation in different ligand systems were investigated herein. Results showed that the critical ROS in both the oxalate and TPP systems are hydroxyl radicals, and that they are produced via one-electron activation of O_2.

Introduction

Zero-valent iron (ZVI) with molecular oxygen can produce reactive oxidants such as the hydroxyl radical (•OH). The mechanisms for •OH production by ZVI and O_2 reaction are as follows (Keenan and Sedlak, 2008; Kim et al., 2015; Joo et al., 2005):

$$Fe^0 + O_2 + 2H^+ \rightarrow H_2O_2 + Fe^{2+} \quad (1)$$

$$Fe^0 + H_2O_2 + 2H^+ \rightarrow Fe^{2+} + 2H_2O \quad (2)$$

$$Fe^{2+} + O_2 \rightarrow Fe^{3+} + \bullet O_2^- \quad (3)$$

* Corresponding author.
E-mail: qincyu@jlu.edu.cn (C. Qin).

https://doi.org/10.1016/j.jes.2020.07.018
1001-0742/

$$Fe^{2+} + \bullet O_2^- + 2H^+ \rightarrow Fe^{3+} + H_2O_2 \quad (4)$$

$$Fe^{2+} + H_2O_2 \rightarrow \bullet OH + Fe^{3+} + OH^- \quad (5)$$

ZVI can be oxidized to produce ferrous ion (Fe(II)) and the hydrogen peroxide (H_2O_2) or H_2O (Eqs. (1) or (2)). Fe(II) oxidation can also be used to produce H_2O_2 (Eqs. (3) and ((4)). H_2O_2 is then activated by Fe(II) to form •OH (Eq. (5)) (Kim et al., 2015). •OH is a strongly reactive oxidant (oxidation potential 2.8 V) in the environment, which can unselectively react with most organics and redox-sensitive elements (Kang et al., 2008; Lee et al., 2013; Zhou et al., 2014).

In recent years, sulfide modification (i.e., "sulfidation") has been of particular interest for improving ZVI reactivity (Tang et al., 2016; Turcio-Ortega et al., 2012). Sulfidated zero-valent iron (SZVI) has a special core-shell structure, covered with a sulfide shell (mainly Mackinawite, FeS). FeS is an effective electronic conductor (Zhang et al., 2016). The FeS shell of SZVI particles conducts delocalized electrons, which can facilitate electron conduction from the core to the surface of ZVI particles, thereby accelerating the reduction of a target substance (Fan et al., 2016). In addition, FeS is relatively hydrophobic; it forms fewer hydroxyl sites than iron oxide and pyrite (FeS_2) (Park et al., 2006; Butler and Hayes, 2001). Researchers have found that the FeS shell can prevent the SZVI from being corroded by water, hence most electrons of the SZVI tend to be transmitted to the target substance, exhibiting electron selectivity (Qin et al., 2018; Lee et al., 2002). Based on these, SZVI is extensively studied and used by researchers and engineers interested in contaminant reduction, including the reduction of nitros, halogenated organics and heavy metals (Song et al., 2017; Fan et al., 2016).

In the presence of dissolved oxygen (DO) or other oxidants, SZVI can be used as a heterogeneous Fenton reagent for the advanced oxidative degradation of organic contaminants, similar to unmodified ZVI. Tang et al. (2016) showed that the oxidation process induced by ZVI can be enhanced by sulfidation, which significantly increases the oxidative degradation rate constant of p-nitrophenol from 0.433 to 1.376 min^{-1} under aerobic conditions at pH 6.77. In the study of oxidative degradation of diclofenac (DCF) under aerobic conditions, Song et al. (2017) discovered that pristine ZVI achieves only 21.2% DCF removal, while the optimal SZVI exhibited 73.5% DCF removal under near neutral conditions (pH 6.5), and the maximum removal reached 85.9% at pH 4.5. Wang et al. (2018) studied Sb(III) removal under aerobic conditions and discovered that the removal rate constant of Sb(III) for pristine ZVI is only 0.005 min^{-1}, while the constant for the optimal SZVI is 0.033 min^{-1}. Overall, the studies on the oxidation properties of SZVI are quite limited, and the related mechanism analysis has not been studied in depth. Furthermore, the difference in sulfidation methods makes this issue much more complicated. For instance, many researchers have their own choices for the S/Fe ratio and sulfidation duration (He et al., 2018; Fan et al., 2017; Hansson et al., 2008). The SZVI preparation method used by Rajajayavel and Ghoshal (2015) was 10 min sonic sulfidation with the Fe/S of 11–50. Han and Yan (2016) rolled the sodium sulfide solution and ZVI on a hematology mixer for 20 min with the S/Fe of 0.00125 to 0.75. The SZVI preparation method of Fan et al. (2016) was rolling on a hematology mixer (15 r/min) for 24 hr with the S/Fe of 0.33–1. The S/Fe ratio and sulfidation duration means the mixing ratio and mixing time of sodium sulfide (or sodium dithionite) solution and ZVI particles, respectively, which determine the content of elemental sulfur on the surface of SZVI. When there is too little S, sulfidation effect is not optimal. Meanwhile, too much S leads to the formation of FeS_2 instead of FeS (Park et al., 2006; Li et al., 2017). Song et al. (2017) proved that the sulfur content of SZVI surface affects the oxidant yield. They pointed out that the abundance of hydroxyl and superoxide radicals increases with an increasing S/Fe ratio, but that when the S/Fe ratio is too high a negative effect is observed.

It is well known that the yield of reactive oxygen species (ROS) in ZVI/O_2 system is low. Although sulfidation improves the yield a little bit, the ROS produced in SZVI/O_2 system remains too low to meet the requirement of actual pollutant degradation (Zhang et al., 2016; Joo et al., 2005). Researchers found that ligands can combine with Fe(II) to form complex (Bernasconi and Baerends, 2008; Zhou et al., 2017), which is beneficial for the production of more ROS for three reasons: (1) ligands can reduce the redox potential of Fe(III)/Fe(II), making the formation of superoxide radicals shown in Eq. (3) more thermodynamically feasible (Welch et al., 2002); (2) under the action of certain ligands, such as polyphosphates, the surface-complexed Fe(III) can obtain electrons from the ZVI core and convert to the surface-complexed Fe(II), that is, a heterogeneous Fe(III)/Fe(II) redox cycle (Li et al., 2014); (3) the complexation of ligands with the surface Fe(II) of ZVI will lead to an increase in the concentration of dissolved Fe(II), which is beneficial for the ROS production. To date, the effect of ligands on the conventional ZVI/O_2 system is widely reported, but the related research on SZVI/O_2 system is rarely involved. Common ligands include organics (such as sodium oxalate, nitrilotriacetic acid, ethylenediaminetetraacetic acid (EDTA)), and inorganics (such as polyphosphate and polyoxometalate), which are widely present in the natural environment (Cao et al., 2016; Lee et al., 2008). A deep understanding of the influence of ligands on oxidative degradation in SZVI/O_2 system is of great necessity for the application of SZVI in the earth's environment.

In this study, tripolyphosphate (TPP) and oxalate were selected as representative inorganic and organic ligands, respectively. The objectives of this study were to explore the characteristics of SnZVI/ligand/O_2 advanced oxidation system. The effects of ligand type and sulfidation content on the reactivity of SnZVI/O_2 system were examined. The mechanisms of free radical generation in this reaction system were also investigated.

1. Materials and methods

1.1. Chemicals

Iron powder (99.9% metals basis, 50 nm) were purchased from the Macklin Biochemical Co., Ltd., Shanghai, China. Ferrous sulfate ($FeSO_4•7H_2O$, 99.0%), sodium tripolyphosphate ($Na_5P_3O_{10}$, 60.0%), sodium oxalate ($Na_2C_2O_4$, 99.8%), benzoic acid (C_6H_5COOH, 99.5%), 1,10-Phenanthroline ($C_{12}H_8N_2•H_2O$, 99.0%), and ethyl alcohol absolute (C_2H_6O, 99.7%) were purchased from the Guangfu Fine Chemical Research Institute, Tianjin, China. Sodium hydroxide (NaOH, 96.0%), hydrochloric acid (HCl, 38.0%), isopropanol (IPA, C_3H_8O, 99.7%) were purchased from the Beijing Chemical Works, Beijing, China. 1,4-Benzoquinone (BQ, $C_6H_4O_2$, 98.0%), and ammonium acetate (CH_3COONH_4, 98.0%) were purchased from the Sinopharm Chemical Reagent Co., Ltd, Beijing, China. Nitrobenzene ($C_6H_5NO_2$, 98.0%), p-nitrophenol ($C_6H_5NO_3$), L-Ascorbic acid (99.7%), sodium sulfide nonahydrate ($Na_2S•9H_2O$, 98.0%), phenol (C_6H_6O, 99.0%), and acetic acid (CH_3COOH, 99.8%) were purchased from the Xilong Science Co., Ltd, Guangdong, China. Acetonitrile (C_2H_3N, HPLC grade, 99.9%) was purchased from Thermo Fisher Scientific, Shanghai, China. Catalase (CAT, bocine liver, BR grade, 2400 u/mg solid) was purchased from the YuanYe Co., Ltd, ShangHai, China. All chemicals were of analytical reagent grade, except for acetonitrile and CAT. All stock solutions were prepared in deionized water.

1.2. nZVI and SnZVI synthesis

All synthesis reactions were carried out under a strictly inert atmosphere in an anaerobic glove box. The nZVI synthesis procedure was as follows: Nanometer iron powder was pretreated with 1 mol/L HCl for 15 sec to remove surface impurities. The iron suspension was then washed with deaerated deionized water (ddw, prepared by deoxygenating deionized water with nitrogen, DO $\leq$ 0.1 mg/L) three times. The obtained slurry was dried in a vacuum oven at 60 °C, then ground and stored in an anaerobic glove box. The resultant powder was used within 3 days.

The SnZVI synthesis procedure was as follows: nZVI suspension (after acid washing) was mechanically vortexed with various concentration of Na_2S aqueous solutions for 1 or 12 hr in a rotary shaker at 150 r/min, marked with S/Fe molar ratios as 0.002, 0.02, 0.1, 0.2 and 0.33, respectively. Afterwards, the resulting SnZVI was washed with ddw three times until its neutral suspension was obtained. Next it was dried in a vacuum oven at 60 °C, ground and stored in an anaerobic glove box. The resultant SnZVI was used within 3 days. The obtained SnZVI are hereinafter referred to as 1h-0.1SnZVI, 1h-0.33SnZVI, 12h-0.002SnZVI, 12h-0.02SnZVI, 12h-0.1SnZVI, and 12h-0.2SnZVI.

1.3. Experimental procedure

Experiments to oxidize phenol and benzoic acid were performed in glass beakers open to the air with mixing at 250 r/min using a propeller type stirrer (DJ1C-120, Jintan Jiangnan Instrument Factory) at 20 ± 5 °C. Air was bubbled (150 mL/min) to keep enough oxygen in the reaction system. After adding the ligand TPP or oxalate to the aqueous solution containing 40 mg/L phenol (or benzoic acid), the initial pH value was adjusted with 1 mol/L HCl and 1 mol/L NaOH solutions. The reaction was initiated by adding 0.1 g nZVI or SnZVI to the reaction solution. Samples taken at intervals were immediately quenched with anhydrous ethanol and then filtered by a 0.22 μm organic needle filter (Nylon 66). It should be pointed out that through experimental verification, the volatilization of phenol and benzoic acid is negligible during the whole experiment.

In the experiment of TPP adsorption by SnZVI, 0.1 g of nZVI or SnZVI was added to 200 mL TPP solution (the concentration is 368 mg/L). The TPP remaining in the solution was measured after mechanical stirring for 1 hr. After adsorption experiments, the SnZVI and nZVI nanoparticles were characterized with Fourier transform infrared spectroscopy (FT-IR).

Various quenching reagents were selectively used to quench different types of ROS. IPA was used to scavenge •OH, and CAT was used to scavenge H_2O_2 produced in the reaction system. Superoxide radical ($\bullet O_2^-$) was scavenged by BQ.

In all the experiments, only the initial pH value was controlled and was done so without adding buffer. This was done in order to avoid the impact of buffer on the experimental system.

1.4. Analytical methods

The phenol concentration was determined by high performance liquid chromatography (HPLC) (Agilent 1100, USA) equipped with an Agilent Eclipse XDB-C18 column (5 μm, 4.6 mm × 250 mm). The column temperature was maintained at 30 °C. The mobile phase of HPLC consisted of a mixture of ultrapure water and acetonitrile (V/V = 50:50) with a total flow rate of 1.0 mL/min. The wavelength was set at 270 nm under ultraviolet detector. The nitrobenzene was analyzed by HPLC consisted of a mixture of 1.0% aqueous acetic acid and acetonitrile (V/V = 45:55) with a total flow rate of 1.0 mL/min, and the wavelength set at 262 nm under ultraviolet detector.

Transmission electron microscopy (TEM, FEI Titan G2 F30) was employed to investigate the structure of the nanoparticles. A fraction of all the samples was freeze-dried for X-ray diffraction (XRD, Bruker D8) and X-ray photoelectron spectrometry (XPS, Escalab 250Xi) analyses. Electron paramagnetic resonance (EPR, Bruker E500) was used to detect •OH and $\bullet O_2^-$, and 5,5-dimethyl-1-pyrroline N-oxide (DMPO) was used as the trapping agent. The determination method of sulfur content is as follows: first, SnZVI was completely dissolved with concentrated hydrochloric acid, and all the S elements were present in the form of H_2S. After that, KBH_4 was added to generate a large amount of H_2 gas, which would carry H_2S gas into a NaOH absorption solution. 0.5% H_2O_2 was added to NaOH absorption solution to oxidize S^{2-} to SO_4^{2-}. Finally, we determined SO_4^{2-} by a Dionex ICS-2100 ion chromatography system to calculate the actual sulfur content. In the process of determining the actual sulfur content of SnZVI, in order to avoid acidification causing the element S to escape in the form of H_2S, a device for collecting H_2S gas was installed (Appendix A Fig. S1).

Total dissolved iron and ferrous ions were detected (absorbance measurement at 510 nm) by the 1,10-phenanthroline spectrometric method. Potassium permanganate titrimetric method was used for the determination of oxalate. The acidic environment was adjusted with 3 mol/L sulfuric acid, and then the oxalate concentration of the sample was titrated with 20 mmol/L potassium permanganate. The TPP in solution was detected by ion chromatography system. The TPP on the nZVI and SnZVI surfaces were detected by FT-IR (Nicolet is5, Thermo Fisher, USA). The solution pH/ORP was analyzed using a pH/ORP meter from Shanghai San-Xin Instrumentation, Inc. (SX721, China). DO was monitored by a dissolved oxygen meter (sensION+DO6, USA).

2. Results and discussions

2.1. Characterization of nZVI and SnZVI particles

TEM images of nZVI, 1h-SnZVI and 12h-SnZVI are shown in Appendix A Fig. S2. The particle sizes are mainly in the range of 50–100 nm. As shown in Appendix A Fig. S2c–S2f, the surface of 12h-SnZVI particles was rougher than that of 1h-SnZVI particles because of the longer sulfidation duration. The 12h-SnZVI particles were covered by some flakes, which were reported as FeS_x in relevant study (Song et al., 2017). The XRD spectra of nZVI and 1h-SnZVI are shown in Appendix A Fig. S3. These particles were detected as iron (syn) crystals, without the presence of iron oxide. XPS measurements of SnZVI samples show peaks for S, demonstrating the presence of S upon sulfidation (Fig. 1). Furthermore, the S^{2-}content of 12h-0.1SnZVI was significantly higher than that of 1h-0.1SnZVI. The XPS results of Fe element of SnZVI (Appendix A Fig. S4) exhibit distinct Fe^{2+} peaks indicating the formation of FeS.

The actual sulfur content (described as the molar ratio of $[S/Fe]_{actual}$, different from $[S/Fe]_{theoretical}$, the theoretical material molar ratio in the synthesis) of each SnZVI was determined by ion chromatography system. The $[S/Fe]_{actual}$ of 1h-0.1SnZVI, 1h-0.33SnZVI, 12h-0.002SnZVI, 12h-0.02SnZVI, 12h-0.1SnZVI and 12h-0.2SnZVI are 0.38 mol%, 1.08 mol%, 0.15 mol%, 1.23 mol%, 4.61 mol% and 6.06 mol%, respectively. Different sulfur contents necessarily lead to different electron transfer efficiency of the FeS shell. We conducted a nitrobenzene anaerobic reduction experiment to determine the electron transfer efficiency of different SnZVIs. As shown in Appendix A Fig. S5, it was found that nitrobenzene degradation efficiency by 12h-0.2SnZVI, 12h-0.1SnZVI, and 12h-0.02SnZVI were all higher than 50%, which were significantly

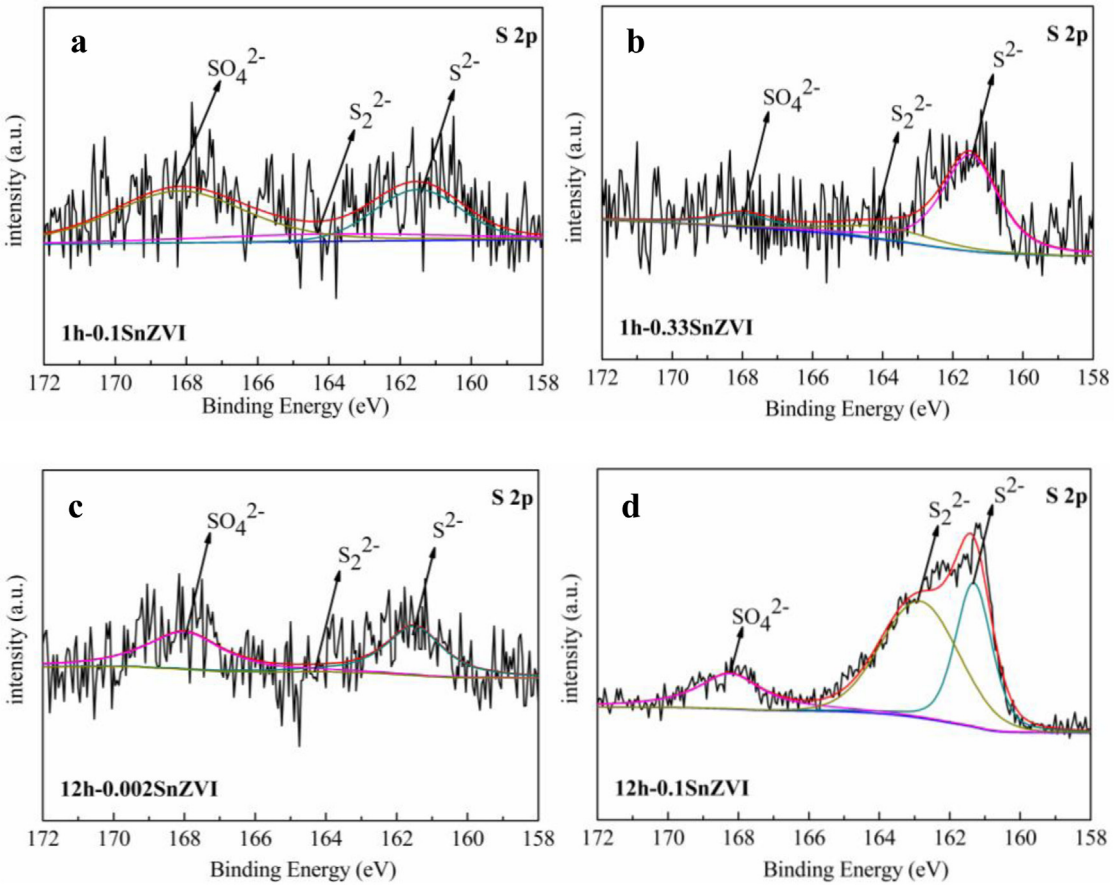

Fig. 1 – Detailed XPS survey of the region for S(2p) for 1h-0.1SnZVI (a), 1h-0.33SnZVI (b), 12h-0.002SnZVI (c) and 12h-0.1SnZVI (d).

higher than that by 1h-0.1SnZVI, 1h-0.33SnZVI, and 12h-0.002SnZVI. Based on the results of reduction experiment, as well as the $[S/Fe]_{actual}$ in each SnZVI, we defined "high sulfur content" as higher than 1.08 mol%, "low sulfur content" as not higher than 1.08 mol%. The SnZVI with a high sulfur content has a better electron transfer ability, which leads to the better nitrobenzene degradation. In addition, hereinafter, 1h-SnZVIs and 12h-0.002SnZVI are collectively referred to as "low-sulfur nZVI", and 12h-SnZVIs other than 12h-0.002SnZVI are collectively referred to as "high-sulfur nZVI".

2.2. *Influence of ligand addition on phenol oxidation in the SnZVI/O_2 system*

Phenol was selected as the target pollutant to conduct this series of experiments. It can be seen from Fig. 2 that phenol was hardly oxidized in the SnZVI/O_2 system without ligand (Fig. 2a and b). We found that the removal rate of phenol in the TPP system was higher than those in the oxalate system within 80 min of reaction at different ligand doses. For instance, the lowest final removal rate (70.1%) in the TPP system is higher than the highest final removal rate (70.0%) in the oxalate system. The advantages of TPP over oxalate are mainly due to its inorganic properties and stronger complexing performance: firstly, the organic ligand is problematic with chemical oxidation applications due to issues such as the scavenging of oxidants and the subsequent self-destruction by oxidation, but the inorganic ligand does not (Kim et al., 2015); secondly, TPP is more effective than oxalate in decreasing the redox potential of Fe(III)/Fe(II) (Li et al., 2014); thirdly, in our subsequent experiments, it was found that the complexation of ligand with surface Fe can promote the dissolution of ionic Fe(II), and that TPP is more effective than oxalate. To investigate the degradation of oxalate during treatment processes, we performed a phenol removal experiment in a dissolved Fe^{2+}/oxalate/O_2 system avoiding the adsorption of oxalate by SnZVI particles. While degrading 37.6% phenol, oxalate was just degraded by 2.5% (Appendix A Fig. S6). The remaining amount of oxalate is still sufficient for catalytic reaction during the following experiment, so the effect of oxalate degradation on phenol degradation is limited.

For the phenol degradation with TPP, the lowest removal rate was 70.1% with an TPP concentration of 1 mmol/L. While for the other reaction systems with higher TPP concentrations, the final phenol removals were almost the same, reaching about 90.0% within 80 min (Fig. 2b). The above experiments were repeated using oxalate instead of TPP. The final phenol removal rates were 52.0%, 70.0%, 50.1%, and 47.6%, respectively, as the concentration of oxalate increased from 5 to 35 mmol/L. A higher concentration of oxalate does not mean a better removal performance, because extra oxalate competes with phenol for ROS.

2.3. *Effect of sulfidation on phenol oxidation in the SnZVI/Oxalate/O_2 system*

As discussed above, phenol was hardly oxidized by SnZVI without ligand. While in the presence of ligands, the

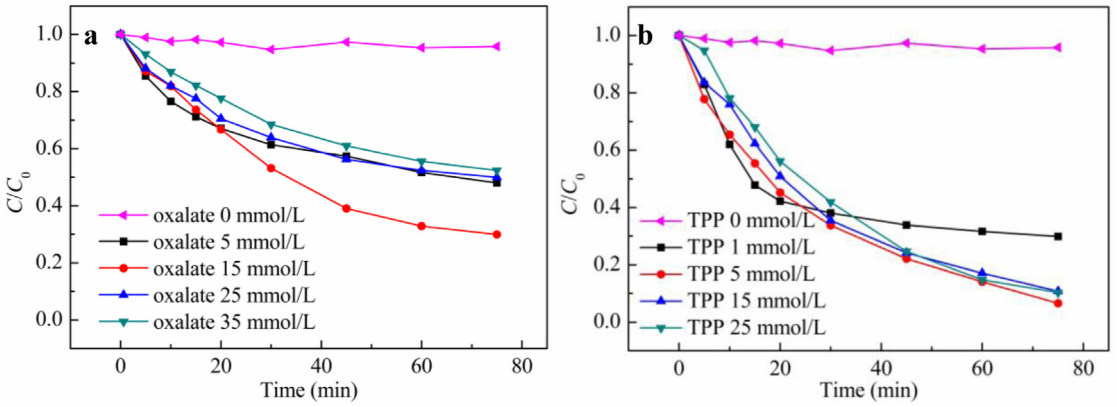

Fig. 2 – Phenol degradation by 1h-0.1SnZVI with different doses of oxalate (a), and TPP (b) under aerobic conditions. Reaction conditions: SnZVI 0.5 g/L, phenol 40 mg/L, initial pH 3.

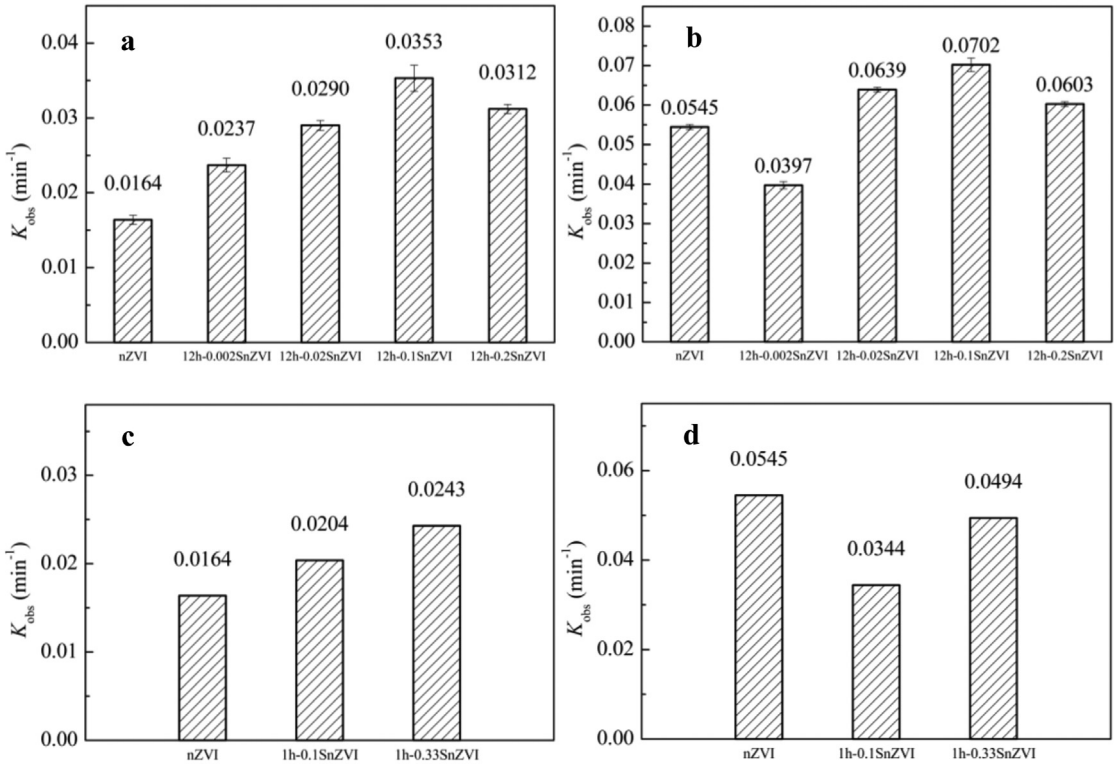

Fig. 3 – The phenol degradation apparent rate constant (K_{obs}) in the 12h-SnZVI/oxalate/O_2 system (a), 12h-SnZVI/TPP/O_2 system (b), 1h-SnZVI/oxalate/O_2 system (c), and 1h-SnZVI/TPP/O_2 system (d) under aerobic conditions. Reaction conditions: SnZVI 0.5 g/L, phenol 40 mg/L, initial pH 3, and ligand 15 mmol/L.

SnZVI oxidation performance varied with the sulfur content (Appendix A Fig. S7a, S8a, S9a and S10a). In order to investigate the effect of sulfidation on the kinetics of phenol degradation, a kinetic model was applied. Due to the solid-liquid inter-phase reaction, the pseudo-first-order kinetic model was utilized. A plot of natural logarithmic C_t/C_0 versus the treatment time is shown in Appendix A Fig. S7b, S8b, S9b and S10b. According to Appendix A Fig. S7b, S8b, S9b and S10b, the apparent rate constants (K_{obs}) of the phenol degradation of each group were obtained, as shown in Fig. 3. Comparing the K_{obs} in Fig. 3a and c, we can find that the phenol removal by high-sulfur nZVI is generally faster than when there is low-sulfur nZVI in the oxalate system. In the 12h-SnZVI/oxalate/O_2 system, it was found that the K_{obs} increased first (0.0237, 0.0290, and 0.0353) and then decreased (0.0353 and 0.0312) with the increase of sulfidation amount. The optimal conditions were 12h-0.1SnZVI (Fig. 3a). The phenol removal rate for 12h-0.1SnZVI within 80 min of reaction is also optimal (78.0%) (Appendix A Fig. S7). While for the 1h-SnZVIs, the K_{obs} (min^{-1}) continuously increased with the increment of sulfidation content (Fig. 3c). It is conceivable that an optimal S content for 1 hr sulfidation would also be obtained as the S content increased to a higher range. In addition, in the oxalate system, all the 12h-SnZVIs and 1h-SnZVIs are more efficient

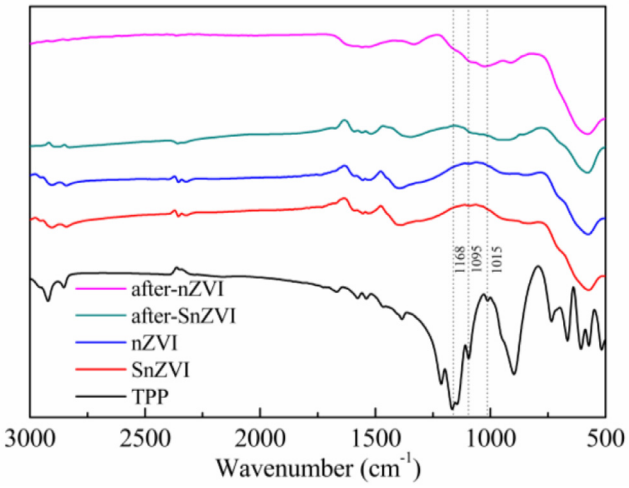

Fig. 4 – FT-IR spectra of nZVI and SnZVI nanoparticles before and after the TPP adsorption.

than nZVI for phenol oxidation. This means that sulfidation is a feasible way to enhance the ZVI/organic ligand/O_2 system.

2.4. *Effect of sulfidation on phenol oxidation in the SnZVI/TPP/O_2 system*

As shown in Fig. 3b, for the phenol removal by 12h-SnZVI in the presence of TPP, the trend of K_{obs} can be described as an initial increase (0.0545, 0.0639, and 0.0702) and then a decrease (0.0702 and 0.0603). This trend is generally similar to that in the oxalate system. An exception is the K_{obs} for 12h-0.002SnZVI, which is lower than that for the nZVI. The K_{obs} for 1h-SnZVI, as shown in Fig. 3d, are also lower than that for the nZVI. This means that the reactivity of low-sulfur nZVI in the presence of TPP is weaker than that of nZVI. To further confirm this distinctive experimental finding, we carried out supplementary experiments with different concentrations of TPP; just as shown in Appendix A Fig. S11, the same pattern of results was obtained in the supplementary experiments. We also selected benzoic acid instead of phenol to duplicate this series of experiments; the reactivity of low-sulfur nZVI on benzoic acid oxidation in the presence of TPP was also weaker than that of nZVI (Appendix A Fig. S12). We explore the reasons for the unexpected results of low-sulfur nZVI/TPP/O_2 systems in Section 2.5.

2.5. *Influence mechanisms of ligands on the contaminant degradation in the low-sulfur nZVI/O_2 system*

We discovered that the reactivity of low-sulfur nZVI in the presence of TPP is weaker than that of nZVI. There is a speculation that it may be due to the weak combination of TPP and FeS shell. In order to confirm this speculation, the change in TPP content both in the solution and on the SnZVI particles surface should be measured.

We determined the change in TPP concentration before and after a TPP adsorption experiment by low-sulfur nZVI (1h-0.33SnZVI) and nZVI, respectively. The results showed that TPP residual concentration in nZVI system is slightly less: it was changed from 360 mg/L before adsorption to 42.23 mg/L after adsorption, while in the low-sulfur nZVI system, it was changed to 45.14 mg/L. After the TPP adsorption experiments, the nZVI and low-sulfur nZVI nanoparticles were characterized with FT-IR (Fig. 4). We found higher P-O stretching vibration peaks on the nZVI surface in the region (Efimov et al., 1997) from 1015 to 1168 cm^{-1}, which means that more TPP is absorbed on the nZVI. Overall, it was confirmed that the combination of TPP and low-sulfur nZVI is indeed weaker than that of TPP and nZVI.

The weak combination of TPP and FeS shell will slow the dissolution of Fe(II) promoted by complexation. We determined the concentration of dissolved iron in each system within 30 min. During the determination, we found that little Fe^{2+} was detected. So we just determined the total iron concentration (including Fe^{2+} and Fe^{3+}). The low concentration of Fe^{2+} was mainly due to its rapid reaction with oxygen in the presence of ligands. The production of Fe^{3+} in the solution is mainly due to the oxidation of Fe^{2+} dissolved from nZVI or SnZVI. The amount of Fe^{3+} directly dissolved from nZVI or SnZVI should be very small, because the surface-complexed Fe(III) can obtain electrons from the ZVI core and convert to the surface-complexed Fe(II) (Li et al., 2014). As shown in Fig. 5b, in the TPP system, the higher the sulfur content of nZVI, the slower the dissolution rate of total Fe. The total dissolved Fe from nZVI, 1h-0.1SnZVI and 1h-0.33SnZVI are 240, 200, 160 mg/L, respectively within 30 min. So nZVI has the best dissolution ability of Fe. While for the oxalate system, the trend is not as remarkable as that in TPP system (Fig. 5a). The total dissolved Fe from nZVI, 1h-0.1SnZVI and 1h-0.33SnZVI are all almost 160 mg/L within 30 min. These results indicate that the weak combination of TPP and FeS shell will inhibit the dissolution of Fe(II) and reduce the ROS induced by dissolved Fe^{2+}.

In addition to the ROS produced by dissolved complexed Fe(II), the surface bound complexed Fe(II) of ZVI also produces ROS (Kim et al., 2015; Zhou et al., 2014; Li et al., 2014). Based on the total dissolved Fe in each system, we set up a series of liquid phase reaction systems with the addition of corresponding amounts of $FeSO_4 \cdot 7H_2O$ to evaluate the contribution of phenol removal by dissolved Fe^{2+} vs. surface bound Fe(II) (Fig. 5c and d). Through calculation, the degradation contributions of surface bound Fe(II) of nZVI, 1h-0.1SnZVI and 1h-0.33SnZVI account for 8.78, 5.45 and 14.38 mg/L, respectively within 30 min in the TPP system. In terms of degradation contributions of surface bound Fe(II), 1h-0.1SnZVI is lower than nZVI, which means that the yield of ROS induced by the surface bound TPP-complexed Fe(II) will decrease due to the weak combination of TPP and FeS shell. While the degradation contributions of surface bound Fe(II) of 1h-0.33SnZVI is higher than that of nZVI. This is because even if the complexation of TPP and FeS is suppressed, the FeS shell promotes electron transfer and thus promotes degradation, which is more apparent on SnZVI with higher sulfur content. In the oxalate system, the degradation contributions of surface bound Fe(II) of nZVI, 1h-0.1SnZVI and 1h-0.33SnZVI account for 0.92, 6.80 and 11.07 mg/L, respectively within 30 min, which means that the benefit of FeS shell play the major role.

In TPP system, the irregularity of the effect of phenol degradation induced by low-sulfur nZVI and high-sulfur nZVI indicates that the sulfidation has a dual effect on degradation reaction. The sulfidation weakens the complexation of TPP with surface bound Fe(II), inhibiting the Fe^{2+} dissolution; meanwhile, proper sulfidation can promote electron transfer from ZVI to oxygen. In contrast, in the oxalate system, sulfidation does not weaken the complexation of oxalate with surface bound Fe(II). Therefore, it only serves to improve the electron transfer.

2.6. *Mechanism of ROS production*

We performed a series of free radical scavenging experiments to investigate the production of ROS in the SnZVI/(TPP or oxalate)/O_2 system. We added IPA to scavenge hydroxyl radical (•OH) produced in the reaction system, CAT to scavenge

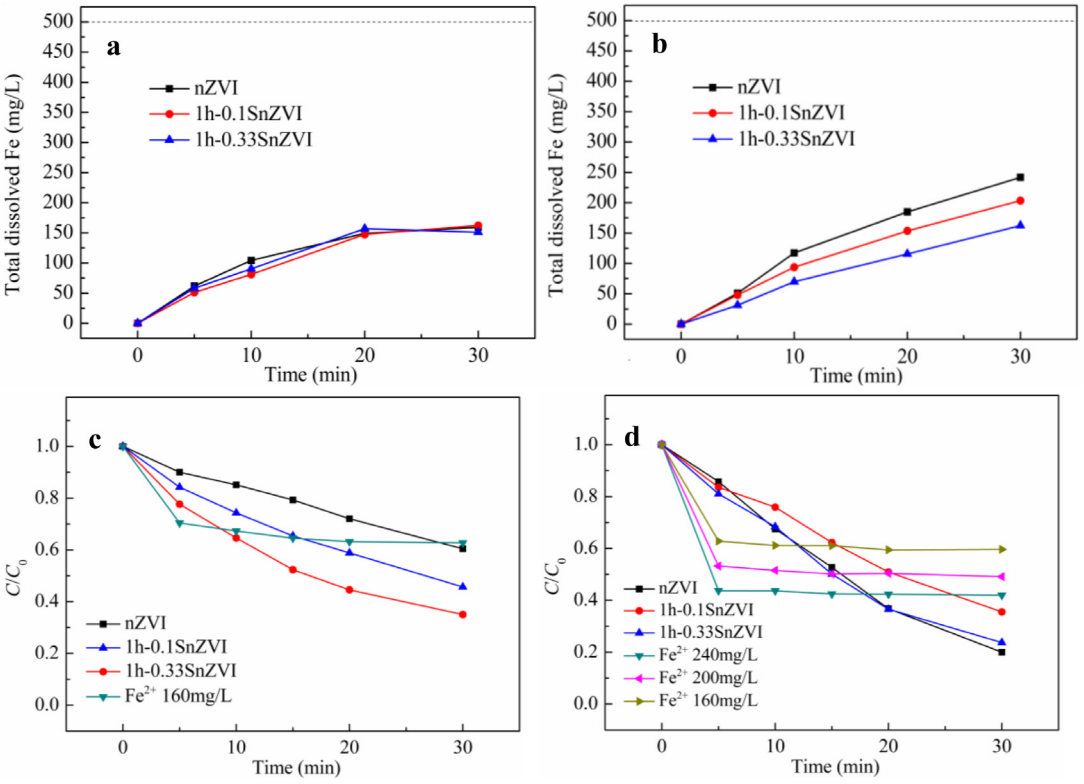

Fig. 5 – Dissolution of Fe from nZVI in a 15 mmol/L oxalate system (a) and a 15 mmol/L TPP system (b). The dashed horizontal black lines represent theoretical maximum dissolved Fe production based on the initial nZVI content. Degradation of phenol by various nZVI and corresponding amount of $FeSO_4 \cdot 7H_2O$ in a 15 mmol/L oxalate system (c) and a 15 mmol/L TPP system (d). Reaction conditions: SnZVI or nZVI 0.5 g/L, phenol 40 mg/L, initial pH 3.

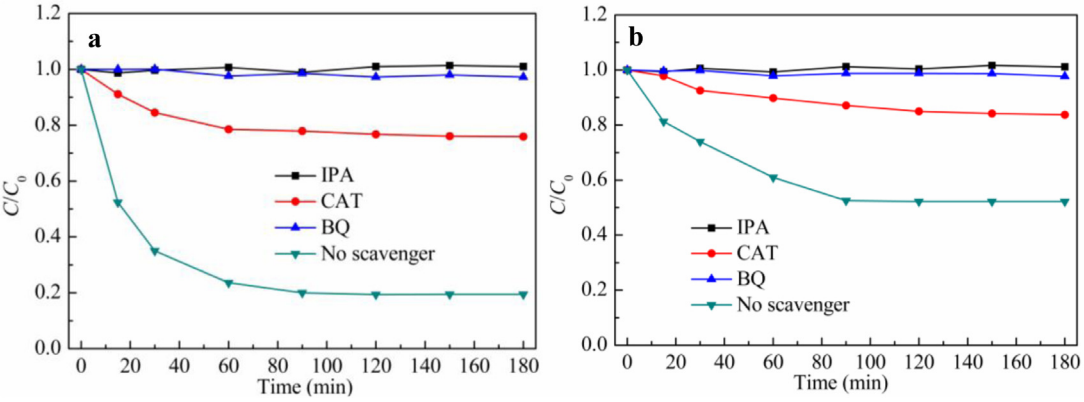

Fig. 6 – Free radical scavenging in the oxalate (a) and TPP (b) systems. Reaction conditions: 1h-0.33SnZVI 0.5 g/L, oxalate 15 mmol/L or TPP 0.5 mmol/L, phenol 40 mg/L, initial pH 3.

hydrogen H_2O_2, BQ to scavenge $\bullet O_2^-$. As shown in Fig. 6a and b, IPA completely inhibits the aerobic degradation of phenol in both ligand systems. This confirms that •OH is the main cause of contaminant degradation. In the presence of CAT, 70.1% of the phenol degradation in the oxalate system was inhibited (Fig. 6a), and 66.0% of the phenol degradation in the TPP system was inhibited (Fig. 6b). This means that H_2O_2 is an intermediate in the production of •OH. We have verified that CAT can completely block the aerobic degradation of phenol in the homogeneous liquid $FeSO_4 \cdot 7H_2O$/TPP/O_2 system, which means that CAT can completely remove H_2O_2 in solution (Appendix A Fig. S13). Therefore, we consider that in the SnZVI/(TPP or oxalate)/O_2 system, the insufficient CAT scavenging effect is due to the H_2O_2 adsorbed on the solid surface of iron particles, which can cause the heterogeneous contaminant degradation without the influence of CAT. As we know, H_2O_2 may be generated by the two-electron transfer ($O_2 \rightarrow H_2O_2$) or the sequential one-electron transfer ($O_2 \rightarrow \bullet O_2^- \rightarrow H_2O_2$) route. In order to determine the electron transfer route, BQ was employed to scavenge $\bullet O_2^-$. As shown in Fig. 6a and b, BQ completely inhibited the aerobic degradation of phenol, which confirms the sequential one-electron

transfer route ($O_2 \rightarrow \bullet O_2^- \rightarrow H_2O_2 \rightarrow \bullet OH$) in both the oxalate and TPP systems.

To further confirm the existence of $\bullet O_2^-$ and •OH in this system, we conducted an electron paramagnetic resonance testing. We selected the 12h-0.1SnZVI/TPP/O_2 system as this experimental system. After 5 min of reactions, characteristic peaks of $\bullet O_2^-$ and •OH were detected (Appendix A Fig. S14). This result more directly demonstrated the existence of $\bullet O_2^-$ and •OH (Zhang et al., 2019).

3. Conclusion

In this study, the addition of ligands was proven to be a remarkably efficient enhancement method for SnZVI induced oxidation. The effective removal of organic contaminants in real water by this SnZVI/O_2/ligand system could be achieved (Appendix A Fig. S15). The studied inorganic ligand (TPP) was more effective than the studied organic ligand (oxalate) to enhance contaminant degradation. In different ligand systems, sulfidation exhibits different effects on the contaminant removal. In the organic ligand system, sulfidation mainly shows an enhanced effect due to the excellent electron transfer ability of FeS shell of SnZVI. In the inorganic ligand systems, due to the hydrophobic character of FeS, the FeS shell hinders the complexation of TPP with surface bound Fe(II), which reduces the dissolution of ferrous ions. Therefore, to some extent, sulfidation has a negative effect on oxidation of contaminants. In view of the hydrophobicity and excellent electron transfer ability of FeS shell, sulfidation could have a dual effect on SnZVI induced oxidation in inorganic ligand systems. With low-sulfur content, sulfidation mainly shows an inhibitory effect, while with the high-sulfur content, enhancement effect plays the major role. These findings show that sufficient S/Fe ratio and duration time are necessary for enhancement of aerobic degradation by SnZVI, especially in inorganic ligand systems. However, it should also be noted that excessive sulfidation will lead to the formation of FeS_2, which should be avoided due to its low electron transfer ability. The mechanism of ROS production is consistent in both organic and inorganic systems. •OH generated by the one-electron activation of O_2 is the main ROS for contaminant degradation. The main significance of this study is to provide some theoretical support for the future application of SnZVI in advanced oxidation.

Acknowledgments

This work was supported by the National Key R&D Program of China (No. 2018YFC1802500), the Key Project of National Natural Science Foundation of China (No. 41530636) and “the Fundamental Research Funds for the Central Universities” .

Appendix A Supplementary data

Supplementary material associated with this article can be found, in the online version, at doi:10.1016/j.jes.2020.07.018.

REFERENCES

Bernasconi, L., Baerends, E.J., 2008. Generation of ferryl species through dioxygen activation in iron/EDTA systems: a computational study. Inorg. Chem. 48 (2), 527–540.

Butler, E.C., Hayes, K.F., 2001. Factors influencing rates and products in the transformation of trichloroethylene by iron sulfide and iron metal. Environ. Sci. Technol. 35 (19), 3884–3891.

Cao, M., Ye, Y., Chen, J., Lu, X., 2016. Remediation of arsenic contaminated soil by coupling oxalate washing with subsequent ZVI/Air treatment. Chemosphere 144, 1313–1318.

Efimov, A.M., 1997. IR fundamental spectra and structure of pyrophosphate glasses along the 2ZnO•P2O5-2Me2O•P2O5 join (Me being Na and Li). J. Non-Cryst. Solids 209 (3), 209–226.

Fan, D., Lan, Y., Tratnyek, P.G., Johnson, R.L., Filip, J., O'Carroll, D.M., et al., 2017. . Sulfidation of iron-based materials: a review of processes and implications for water treatment and remediation. Environ. Sci. Technol. 51 (22), 13070–13085.

Fan, D., O'Brien Johnson, G, Tratnyek, P.G, Johnson, R.L, 2016. Sulfidation of nano zerovalent iron (nZVI) for improved selectivity during in-situ chemical reduction (ISCR). Environ. Sci. Technol. 50 (17), 9558–9565.

Han, Y., Yan, W., 2016. Reductive dechlorination of trichloroethene by zero-valent iron nanoparticles: reactivity enhancement through sulfidation treatment. Environ. Sci. Technol. 50 (23), 12992–13001.

Hansson, E., Odziemkowski, M., Gillham, R., 2008. Influence of Na2S on the degradation kinetics of CCl4 in the presence of very pure iron. J. Contam. Hydrol. 98 (3–4), 128–134.

He, F., Li, Z., Shi, S., Xu, W., Sheng, H., Gu, Y., et al., 2018. Dechlorination of excess trichloroethene by bimetallic and sulfidated nanoscale zero-valent iron. Environ. Sci. Technol. 52 (15), 8627–8637.

Joo, S.H., Feitz, A.J., Sedlak, D.L., Waite, T.D., 2005. Quantification of the oxidizing capacity of nanoparticulate zero-valent iron and assessment of possible environmental applications. Environ. Sci. Technol. 39 (5), 1263–1268.

Kang, S.H., Choi, W., 2008. Oxidative degradation of organic compounds using zero-valent iron in the presence of natural organic matter serving as an electron shuttle. Environ. Sci. Technol. 43 (3), 878–883.

Keenan, C.R., Sedlak, D.L., 2008. Ligand-enhanced reactive oxidant generation by nanoparticulate zero-valent iron and oxygen. Environ. Sci. Technol. 42 (18), 6936–6941.

Kim, H.H., Lee, H., Kim, H.E., Seo, J., Hong, S.W., Lee, J.Y., et al., 2015. Polyphosphate-enhanced production of reactive oxidants by nanoparticulate zero-valent iron and ferrous ion in the presence of oxygen: yield and nature of oxidants. Water Res. 86, 66–73.

Lee, C., Keenan, C.R., Sedlak, D.L., 2008. Polyoxometalate-enhanced oxidation of organic compounds by nanoparticulate zero-valent iron and ferrous ion in the presence of oxygen. Environ. Sci. Technol. 42 (13), 4921–4926.

Lee, H, Lee, H.J, Sedlak, D.L, Lee, C, 2013. pH-Dependent reactivity of oxidants formed by iron and copper-catalyzed decomposition of hydrogen peroxide. Chemosphere 92 (6), 652–658.

Lee, W., Batchelor, B., 2002. Abiotic reductive dechlorination of chlorinated ethylenes by iron-bearing soil minerals. 1. Pyrite and magnetite. Environ. Sci. Technol. 36 (23), 5147–5154.

Li, J., Zhang, X., Sun, Y., Liang, L., Pan, B., Zhang, W., et al., 2017. Advances in sulfidation of zerovalent iron for water decontamination. Environ. Sci. Technol. 51 (23), 13533–13544.

Li, W., Menghua, C., Zhihui, A., Lizhi, Z., 2014. Dramatically enhanced aerobic atrazine degradation with Fe@Fe2O3 core-shell nanowires by tetrapolyphosphate. Environ. Sci. Technol. 48 (6), 3354–3362.

Park, S.W., Kim, S.K., Kim, J.B., Choi, S.W., Inyang, H.I., Tokunaga, S., 2006. Particle surface hydrophobicity and the dechlorination of chloro-compounds by iron sulfides. Water Air Soil Pollut. 6 (1–2), 97–110.

Qin, H., Guan, X., Bandstra, J.Z., Johnson, R.L., Tratnyek, P.G., 2018. Modeling the kinetics of hydrogen formation by zerovalent iron: effects of sulfidation on micro-and nano-scale particles. Environ. Sci. Technol. 52 (23), 13887–13896.

Rajajayavel, S.R.C., Ghoshal, S., 2015. Enhanced reductive dechlorination of trichloroethylene by sulfidated nanoscale zerovalent iron. Water 78, 144–153.

Song, S., Su, Y., Adeleye, A.S., Zhang, Y., Zhou, X., 2017. Optimal design and characterization of sulfide-modified nanoscale zerovalent iron for diclofenac removal. Appl. Catal. B-Environ. 201, 211–220.

Tang, J., Tang, L., Feng, H., Zeng, G., Dong, H., Zhang, C., et al., 2016. . pH-dependent degradation of p-nitrophenol by sulfidated nanoscale zerovalent iron under aerobic or anoxic conditions. J. Hazard. Mater. 320, 581–590.

Turcio-Ortega, D., Fan, D., Tratnyek, P.G., Kim, E.J., Chang, Y.S., 2012. Reactivity of Fe/FeS nanoparticles: electrolyte composition effects on corrosion electrochemistry. Environ. Sci. Technol. 46 (22), 12484–12492.

Wang, Y., Shao, Q., Huang, S., Zhang, B., Xu, C., 2018. High performance and simultaneous sequestration of Cr(VI) and Sb(III) by sulfidated zerovalent iron. J. Clean Prod. 191, 436–444.

Welch, K.D., Davis, T.Z., Aust, S.D., 2002. Iron autoxidation and free radical generation: effects of buffers, ligands, and chelators. Arch. Biochem. Biophys. 397 (2), 360–369.

Zhang, C., Li, T., Zhang, J., Yan, S., Qin, C., 2019. Degradation of p-nitrophenol using a ferrous-tripolyphosphate complex in the presence of oxygen: the key role of superoxide radicals. Appl. Catal. B-Environ. 259, 0926–3373.

Zhang, P., Yuan, S., Liao, P., 2016. Mechanisms of hydroxyl radical production from abiotic oxidation of pyrite under acidic conditions. Geochim. Cosmochim. Acta 172, 444–457.

Zhou, H., Sun, Q., Wang, X., Wang, L., Chen, J., Zhang, J, et al., 2014. Removal of 2,4-dichlorophenol from contaminated soil by a heterogeneous ZVI/EDTA/Air Fenton-like system. Sep. Purif. Technol. 132, 346–353.

Zhou, T., Zou, X., Wu, X., Mao, J., Wang, J., 2017. Synergistic degradation of antibiotic norfloxacin in a novel heterogeneous sonochemical Fe0/tetraphosphate Fenton-like system. Ultrason. Sonochem. 37, 320–327.